


Revolving supramolecular chiral structures powered by light in nanomotor-doped liquid crystals

Tetiana Orlova¹, Federico Lancia², Charles Loussert¹, Supitchaya Iamsaard², Nathalie Katsonis¹ ^{2*} and Etienne Brasselet^{1*}

Molecular machines operated by light have been recently shown to be able to produce oriented motion at the molecular scale^{1,2} as well as do macroscopic work when embedded in supramolecular structures^{3–5}. However, any supramolecular movement irremediably ceases as soon as the concentration of the interconverting molecular motors or switches reaches a photo-stationary state^{6,7}. To circumvent this limitation, researchers have typically relied on establishing oscillating illumination conditions—either by modulating the source intensity^{8,9} or by using bespoke illumination arrangements^{10–13}. In contrast, here we report a supramolecular system in which the emergence of oscillating patterns is encoded at the molecular level. Our system comprises chiral liquid crystal structures that revolve continuously when illuminated, under the action of embedded light-driven molecular motors. The rotation at the supramolecular level is sustained by the diffusion of the motors away from a localized illumination area. Above a critical irradiation power, we observe a spontaneous symmetry breaking that dictates the directionality of the supramolecular rotation. The interplay between the twist of the supramolecular structure and the diffusion¹⁴ of the chiral molecular motors creates continuous, regular and unidirectional rotation of the liquid crystal structure under non-equilibrium conditions.

We use overcrowded alkenes Ph-**m** or Me-**m** as molecular motors (Fig. 1a). Upon illumination, **m** transforms into its unstable isomer **m***, while the reverse transformation **m*** → **m** occurs at room temperature spontaneously. Once these molecular motors are incorporated in an achiral liquid crystal, amplification of chirality yields a photo-responsive cholesteric liquid crystal. This helix-based liquid crystal is further confined between two glass slides, each of them promoting perpendicular orientation of the liquid crystal molecules. When the gap *L* of the cell is typically smaller than the helical pitch *p* of the cholesteric liquid crystal (the distance over which the average molecular orientation of the liquid crystal rotates by 2π , and whose sign defines the handedness of the cholesteric helix), the helix is suppressed¹⁵. This geometrical frustration can be released when energy kicks in locally, by the use of either electric fields¹⁶ or laser beams¹⁷ and yields a variety of complex twisted topological structures¹⁸ that are all characterized by a constant cholesteric pitch.

Here, the geometrical frustration is released by winding the helix mechanically (by the twisting action of the molecular motor) in a system where **m** is combined with a shape-persistent chiral co-dopant (Supplementary Fig. 1). Co-doping is necessary because most photo-responsive chiral dopants induce helical unwinding under

illumination, and here releasing geometrical frustration requires photo-induced winding. By adjusting the relative proportions of motor and shape-persistent co-dopant, as well as their concentrations, we have prepared cholesteric liquid crystals that display opposite helical handedness at full photo-conversion—for example, provided that the illumination is sufficiently strong (Supplementary Table 1). The initial helical pitch p_0 first increases under illumination, and while the motor continues to photo-convert, the cholesteric helix reverses its handedness and starts winding continuously in the opposite direction (Fig. 1a), until it reaches its saturated photo-stationary value p_∞ . We use steady irradiation conditions provided by a focused laser beam at wavelength $\lambda = 375$ nm (Fig. 1b), and observe the system under crossed linear polarizers (Supplementary Fig. 2). In practice, the emergence of any three-dimensional liquid crystal structure is thus assessed by a two-dimensional pattern. In our earlier work, we have shown that the mechanical winding provided by the motors can generate several types of twisted structures, above a minimal power P_{\min} ¹⁹. Here we report on out-of-equilibrium dynamics that occur via a structural transition, when the illumination power is used as a control parameter.

At power values $\sim 1.25P_{\min}$ we can stabilize a twisted liquid crystal structure associated to an axially symmetric and chiral pattern, and that can be either right-handed or left-handed (Fig. 1c,d). Increasing the irradiation power further and up to $\sim 2P_{\min}$ we unveil a breaking in axial symmetry that defines a structural transition: the axial symmetry of the chiral pattern is broken and yields another, much larger chiral pattern that exhibits a kink (Fig. 1e,f), and the handedness of which is pre-determined by the handedness of the axisymmetric pattern (Fig. 1c,d). Strikingly, the emergence of this new pattern is accompanied by its continuous, regular, and unidirectional rotation, in a direction that is pre-determined by its handedness (Supplementary Videos 1,2 and Fig. 2a–c). The fact that the diameter of the beam is three to five times smaller than the diameter of the pattern is a clear manifestation that **m*** diffuses away from the illuminated zone. When the light is turned off, the pattern fades away.

Constant and stable rotation is sustained under steady illumination conditions—up to forty hours of continuous rotation have been observed for both directions of rotation, without any signs of fatigue. Plotting the correlation coefficient between an image observed at any time *t* and a reference image, quantifies the similarity between two images over time (Fig. 2d). The corresponding Fourier spectrum provides a quantitative analysis for the rotation rate (Fig. 2e), and highlights that the revolving elastic excitation is

¹Univ. Bordeaux, CNRS, LOMA, UMR 5798, Talence, France. ²Bio-inspired and Smart Materials, MESA+ Institute for Nanotechnology, University of Twente, Enschede, The Netherlands. *e-mail: n.h.katsonis@utwente.nl; etienne.brasselet@u-bordeaux.fr

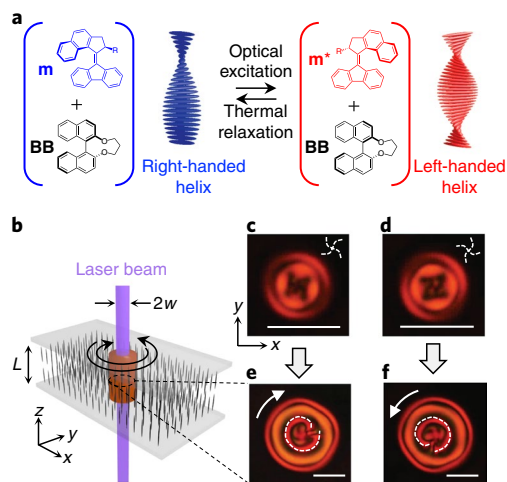


Fig. 1 | Motor-doped liquid crystals winding under irradiation, and associated chiral structures. **a**, Molecular motor used as photo-active dopant, with a substituent R on the stereogenic centre. Two derivatives were used: Ph-**m** (R=phenyl group), and Me-**m** (R=methyl group). A bridged binol **BB** was used as a passive co-dopant. When mixed with a nematic liquid crystal, the dopant and co-dopant generate a photo-responsive cholesteric liquid crystal by combined chirality transfer. Helix inversion is associated both with the photo-isomerization $\mathbf{m} \rightarrow \mathbf{m}^*$, and with its spontaneous reverse transformation $\mathbf{m}^* \rightarrow \mathbf{m}$. **b**, Motor-doped liquid crystal film with thickness $L = 10 \mu\text{m}$ confined between two glass slides promoting perpendicular orientation of the molecules and illuminated locally using a Gaussian laser beam with a beam waist $w = 5 \mu\text{m}$ at wavelength $\lambda = 375 \text{ nm}$. **c, d**, Axisymmetric chiral patterns with opposite handedness observed by polarized optical microscopy between crossed linear polarizers. Such patterns can be sustained for a minimal illumination power of $\sim 1.25 P_{\text{min}}$. The dashed twisted crosses are a guide for the eyes, to identify the broken chiral symmetry in the pattern. **e, f**, A secondary structural symmetry breaking takes place spontaneously as the power increases up to $\sim 2P_{\text{min}}$ and leads to a non-axisymmetric pattern that features a kink. This pattern rotates continuously, and both its handedness and the direction of rotation are predetermined by the axisymmetric pattern from which it results (**c** or **d**). The dashed spirals emphasize the handedness of the pattern and the solid white arrow shows the direction of rotation. Scale bars, $20 \mu\text{m}$.

robust in its operation. Finally, the emergence of rotation is only marginally influenced by ageing, as demonstrated by two rotating structures observed more than three years apart (Supplementary Videos 1,3). Moreover, this rotation does not depend on the polarization of the laser light, and has been observed with both linearly and circularly polarized light.

We have investigated how the rotation rate depends on the use of a given enantiomer of either Ph-**m** or Me-**m**. We conclude that there is a general character to the rotation, as seen in Fig. 3a, where the period of rotation T_0 correlates with the diameter d of any revolving pattern (experimentally, a range of different diameters can be accessed by using different irradiation powers). Specifically, the results evidence an exponential dependence of the rotation period with the diameter of the chiral pattern that is valid for both motors and independently of the direction of rotation. Remarkably, this trend is not compatible with a quadratic law $T_0 \sim d^2/D$ that can be inferred from a dimensional analysis neglecting the ordered nature of the liquid crystal. This exponential dependence thus suggests that, in addition to diffusion, another parameter plays a key role in establishing the rotation, and this is the long-range orientational order that is characteristic for liquid crystals. Further, the rotation rate is influenced by the bulkiness of the substituents at the stereogenic centre; specifically, it has been shown that an increase of steric hindrance speeds up the rotary motion of the molecular motor²⁰. As Me-**m**^{*} relaxes faster than Ph-**m**^{*}, the former motor displays a tendency to generate smaller chiral patterns (squares) than the latter (circles), and smaller diameters are associated with faster pattern rotation. Both enantiomers can lead to clockwise and counter-clockwise rotation, which means that the direction of rotation cannot be predicted by choosing one enantiomer over the other, but is instead pre-programmed at the supramolecular level, as illustrated in Fig. 1c–f. Two enantiomers induce the same rotation rates.

The diameter of the chiral pattern d depends on the incident reduced power P (Fig. 3b). A simple reaction–diffusion model allows one to perform a quantitative analysis of this dependence (see Methods). As frustration is released when the pitch magnitude $|p|$ is below the critical value p_c , in a simple picture this qualitatively means that in the areas where the pattern is formed, $|p| < p_c$. We can thus estimate the diameter of the structure from the condition $|p(d/2)| = p_c$, and further show that the diameters of the patterns

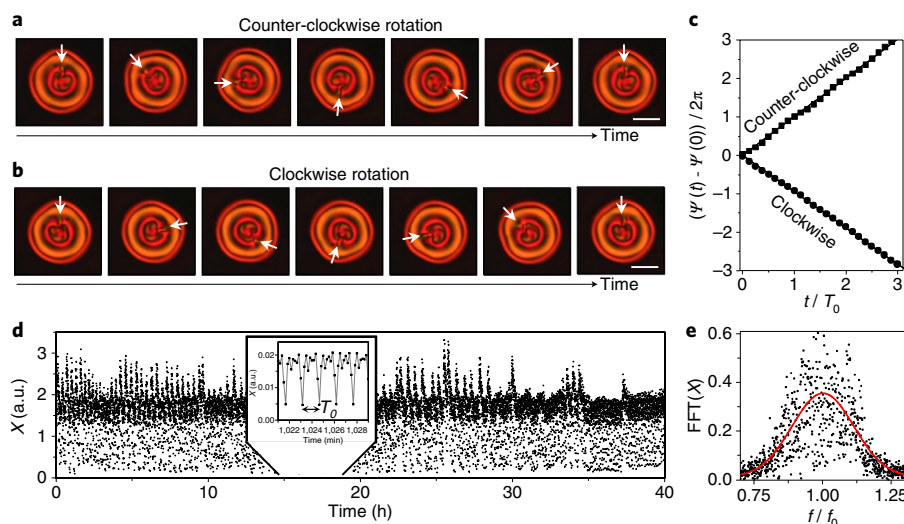


Fig. 2 | Light-driven chiral structures revolving unidirectionally **a, b**, Snapshots of chiral patterns revolving counter-clockwise and clockwise over one period. **c**, The polar angle ψ of the structural kink (see white arrow) in the (x, y) plane is plotted against time. The line refers to the best linear fit of the data. **d**, Correlation coefficient X between any image and the reference image at $t = 0$. The inset evidences a period $T_0 \sim 2 \text{ min}$. **e**, Fourier spectrum of $X(t)$ plotted around the mean rotation frequency $f_0 = 1/T_0$. The red curve is a Gaussian fit. Scale bars, $20 \mu\text{m}$.

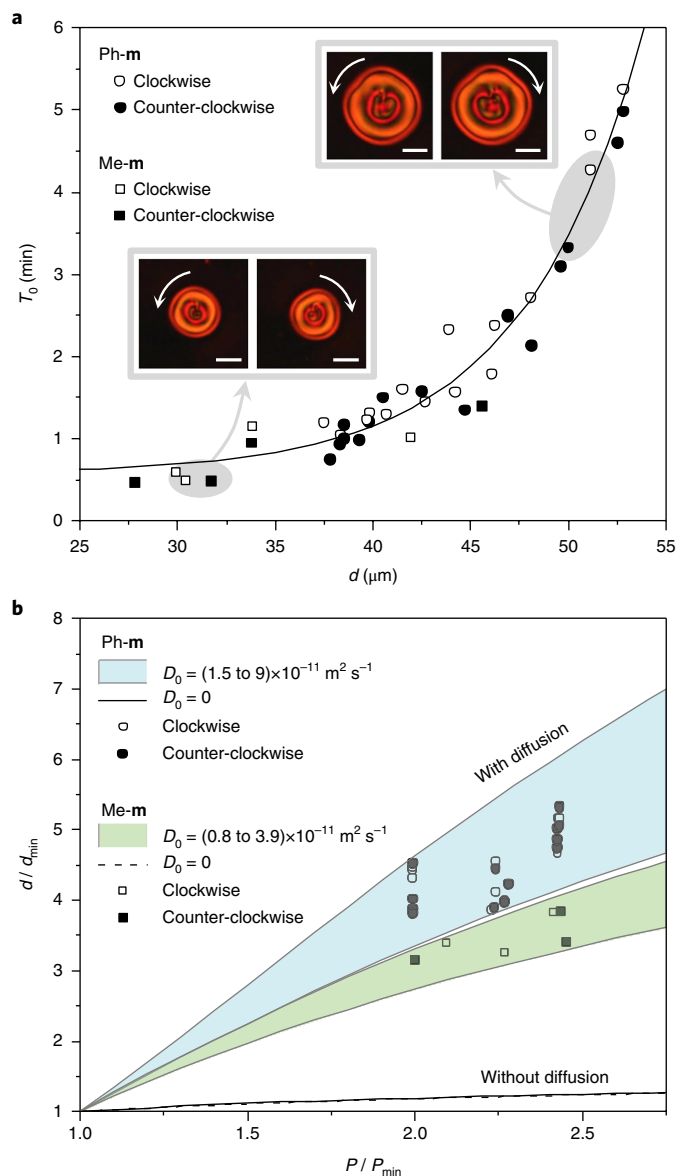


Fig. 3 | Universal character of the revolving chiral structures. a, Rotation period T_0 as a function of the structure diameter d for molecular motors Ph-m and Me-m, and for both clockwise and counter-clockwise rotation. The diameter d is defined experimentally as the diameter of the largest bright ring of the pattern. The solid line refers to an exponential fit. Insets: polarizing microscopy snapshots of revolving chiral patterns obtained with Me-m (squares) and Ph-m (circles). Scale bars, 20 μm . **b**, Dependence of the structure diameter d as a function of the power of the incident ultraviolet laser beam, where d_{min} and P_{min} refer to the smallest stable and static structure. The experimental data are plotted against data extracted from simulations based on a simplified reaction-diffusion model ('with diffusion') and from a purely kinetic model ('without diffusion'), both neglecting the coupling with the twisted three-dimensional liquid crystal structure (see Methods). The diffusion constant is approximated to be the same for all the motors, and is denoted as D_0 . Sample characteristics and individual analysis of each sample are provided in Supplementary Figs. 3 and 4.

that are observed experimentally correspond to diffusion coefficients of the molecular motors $D_0(\text{Ph-m}) \sim 5.25 \pm 3.75 \times 10^{-11} \text{ m}^2 \text{ s}^{-1}$ and $D_0(\text{Me-m}) \sim 2.35 \pm 1.55 \times 10^{-11} \text{ m}^2 \text{ s}^{-1}$. This range of values is in good agreement with literature values²¹ and thus confirms that diffusion is key in the emergence of these structures.

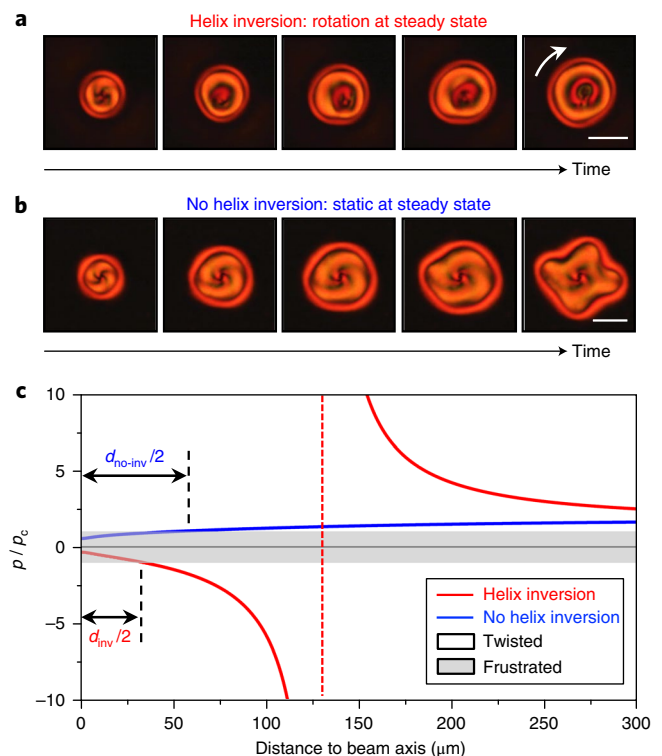


Fig. 4 | Helix inversion promotes spatial confinement, and thus preserves the integrity of the revolving patterns. a, Transient dynamics leading to continuous rotation in the presence of helix inversion (147 s). Scale bars, 20 μm . **b**, Transient dynamics leading to fingerprint pattern formation without cholesteric helix inversion (~75 s). Scale bar, 20 μm . **c**, Simulated dependence of the helix pitch on the distance to the ultraviolet beam axis with d_{inv} and $d_{\text{no-inv}}$ the estimated size of the twisted structures with and without helix inversion, which is derived from the frustration condition $|p(d/2)| = p_c$. Simulation parameters: $p_0 = 16 \mu\text{m}$; $p_\infty = 1.6 \mu\text{m}$; diffusion coefficient, $D_0 = 3.5 \times 10^{-11} \text{ m}^2 \text{ s}^{-1}$; Gaussian beam power, 20 nW (with helix inversion, i.e. $p_\infty = -1.6 \mu\text{m}$) and 5 nW (without helix inversion, i.e. $p_\infty = +1.6 \mu\text{m}$); Gaussian beam waist, $w = 5 \mu\text{m}$.

We also demonstrate that the occurrence of helix inversion plays a key role in preserving the integrity of the light-fuelled rotor. For a cholesteric liquid crystal with a composition that does not allow helix inversion, the axisymmetric structure is destabilized into the outward growth of fingerprints, and the transition to a rotational regime does not occur (Fig. 4a,b and Supplementary Videos 4,5). Moreover, the diameter of the structure in the case of helix inversion is larger than without, which further indicates that helix inversion promotes radial confinement of the liquid crystal reorientation, as supported by our model (Fig. 4c). Indeed, the latter predicts a much steeper pitch increase along the radial coordinate in helix-inverting cholesteric helices, a feature which is associated with a larger elastic energy barrier, and thus makes it difficult for the chiral pattern to grow. This underpins the role of elastic chiral gradients in the emergence of rotation.

The work produced by the revolving structure can be harnessed into the rotation of a particle-like liquid crystal structure, which behaves like an independent object, of diameter $\sim 30 \mu\text{m}$ (Fig. 5 and Supplementary Video 6). Its trapping results from the complex elastic landscape that emerges as a response to the inhomogeneous liquid crystal orientation. In contrast to what was observed in other systems⁶, the rotation speed of the cargo particle equals that of the revolving chiral pattern, the latter being only marginally influenced by the presence of the cargo.

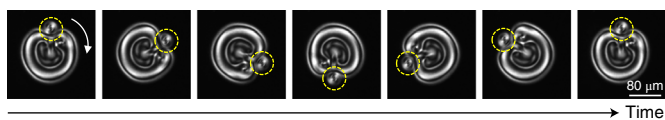


Fig. 5 | Orbital transport of cargo. Off-axis rotational transport of a cargo, here a particle-like liquid crystal structure, being subjected to an orbiting trajectory under the effect of the revolving pattern. The rotation period is ~23 min.

Our experimental findings support a physico-chemical mechanistic understanding of the rotation. Localized illumination of nanomotor-doped liquid crystal in confinement generates toroid-like structures. As long as the axisymmetry of the supramolecular structure is preserved (Fig. 1c,d), the diffusion of chiral motors along gradients of concentrations remains invariant per rotation, and thus it never yields any rotation even when \mathbf{m} and \mathbf{m}^* have different diffusion rates. In contrast, once axial symmetry is broken (Fig. 1e,f), the twist of the medium, and thus the propagation rate of the motors, become angle-dependent. This angular dependence impacts the twist gradients, as a result of the long-range orientational order characterizing liquid crystals, in which a local change of twist also affects neighbouring molecules. The new angular dependence also redefines the angular redistribution of the diffusing motors. This leads to the orthoradial propagation of the non-local excitation, which we detect experimentally as a rotating spiral-shaped pattern. In addition, it is the chiral nature of the non-axisymmetric supramolecular structure that provides the directional character to the liquid crystal reorganization.

Given a physico-chemical perturbation on the spatial scale ℓ , we note that the characteristic elastic relaxation time $\tau_{\text{elast}} = (\gamma/K)\ell^2$ (where γ is the rotational viscosity and K is the typical elastic constant of the liquid crystal, with γ/K equal to a few 10^{10} sm^{-2}) and the characteristic diffusion time $\tau_{\text{diff}} = (1/D_0)\ell^2$ are of the same order of magnitude, which suggests that a feedback mechanism is established, without time delay.

Overall, we propose that the emergence of rotation is based on a non-local feedback loop that involves the local concentrations of \mathbf{m} and \mathbf{m}^* , and their spatial gradients, as well as twist gradients that occur across the liquid crystal structure. Indeed, the diffusion of a chiral species is influenced by the chirality of the liquid crystal in which they diffuse, and vice versa^{22,23}. Therefore, while the spatial distribution of the molecular motors defines the distribution of the pitch, in return, the elastic relaxation and the differential diffusion rates of \mathbf{m} and \mathbf{m}^* define a new chiral landscape (this interplay is illustrated in Supplementary Scheme 1).

Chirality is thus key to the emergence of rotation, and appears to be a universal design principle²⁴, as observed in the directional reorientation of passive liquid crystalline media employing unidirectional transfer of optical angular momentum carried by chiral light to achiral liquid crystals^{25,26} or unidirectional Marangoni flows driven by absorption of light in chiral liquid crystals²⁷. However, the latter systems lack any active molecular component, and therefore they also involve light intensity levels that are at least five orders of magnitude higher than the $\sim 50 \text{ mW cm}^{-2}$ here, which is compatible with sunlight illumination. Another classic example of macroscopic dynamics in chiral liquid crystals is the so-called Lehmann rotation, where chiral liquid crystals are driven by a gradient of temperature along the helical axis²⁸, and which remains an intriguing phenomenon to date²⁹. The same mechanism yields molecular precession of a chiral liquid-crystalline monolayer spread on a glycerol surface; however, this precession remains short-lived³⁰.

By engineering reaction–diffusion processes in a medium characterized by long-range orientational order and taking advantage of large chiral gradients, we demonstrate the emergence of revolving structures, in a phenomenon that appears as a supramolecular and

chiral counterpart of the Belousov–Zhabotinsky reaction. These chiral supramolecular structures maintain non-equilibrium conditions at length scales which are typically 10,000 times larger than their individual components. These results contribute to developing autonomous molecular systems that are capable of transforming light into work continuously.

Methods

Methods, including statements of data availability and any associated accession codes and references, are available at <https://doi.org/10.1038/s41565-017-0059-x>.

Received: 6 September 2017; Accepted: 20 December 2017;

Published online: 12 February 2018

References

- Balzani, V., Credi, A. & Venturi, M. Light powered molecular machines. *Chem. Soc. Rev.* **38**, 1542–1550 (2009).
- Kassem, S. et al. Artificial molecular motors. *Chem. Soc. Rev.* **46**, 2592–2621 (2017).
- Browne, W. R. & Feringa, B. L. Making molecular machines work. *Nat. Nanotech.* **1**, 25–35 (2006).
- Chen, J. et al. Artificial muscle-like function from hierarchical supramolecular assembly of photoresponsive molecular motors. *Nat. Chem.* <https://doi.org/10.1038/nchem.2887> (2017)
- Van Leeuwen, T., Lubbe, A. S., Stacko, P., Wezenberg, S. J. & Feringa, B. L. Dynamic control of function by light-driven molecular motors. *Nat. Rev. Chem.* **1**, 0096 (2017).
- Eelkema, R. et al. Molecular machines: Nanomotor rotates microscale objects. *Nature* **440**, 163 (2006).
- Li, Q. et al. Macroscopic contraction of a gel induced by the integrated motion of light-driven molecular motors. *Nat. Nanotech.* **10**, 161–165 (2015).
- Foy, J. T. et al. Dual-light control of nanomachines that integrate motor and modulator subunits. *Nat. Nanotech.* **12**, 540–545 (2017).
- Yamada, M. et al. Photomobile polymer materials: Towards light-driven plastic motors. *Angew. Chem. Int. Ed.* **47**, 4986–4988 (2008).
- Gelebart, A. H. et al. Making waves in a photoactive polymer film. *Nature* **546**, 632–636 (2017).
- White, T. J. et al. A high frequency photodriven polymer oscillator. *Soft Matter* **4**, 1796–1798 (2008).
- Tabe, Y. et al. Photo-induced travelling waves in condensed Langmuir monolayers. *New J. Phys.* **5**, 65.1–65.11 (2011).
- Martinez, A. & Smalyukh, I. I. Light-driven dynamic Archimedes spirals and periodic oscillatory patterns of topological solitons in anisotropic soft matter. *Opt. Express* **23**, 4591–4604 (2015).
- Epstein, I. R. & Xu, B. Reaction–diffusion processes at the nano and micro scales. *Nat. Nanotech.* **11**, 312–319 (2016).
- Zeldovich, B. Y. & Tabiry, N. V. Fréedericksz transition in cholesteric liquid crystal without external fields. *JETP Lett.* **34**, 406–408 (1981).
- Haas, W. E. L. & Adams, J. E. Electrically variable diffraction in spherulitic liquid crystals. *Appl. Phys. Lett.* **25**, 263–264 (1974).
- Smalyukh, I. I. et al. Three-dimensional structure and multistable optical switching of triple-twisted particle-like excitations in anisotropic fluids. *Nat. Mater.* **9**, 139–145 (2010).
- Ackerman, P. J. et al. Two-dimensional skyrmions and other solitonic structures in confinement-frustrated chiral nematics. *Phys. Rev. E* **90**, 012505 (2014).
- Loussert, C. et al. Subnanowatt opto-molecular generation of localized defects in chiral liquid crystals. *Adv. Mater.* **26**, 4242–4246 (2014).
- Vicario, J., Walko, M., Meetsma, A. & Feringa, B. L. *J. Am. Chem. Soc.* **128**, 5127–5135 (2006).
- Pumpa, M. & Cichos, F. Slow single-molecule diffusion in liquid crystals. *J. Phys. Chem. B* **116**, 14487–14493 (2012).
- Galstian, T. & Allahverdyan, K. Molecular self-assemblies might discriminate the diffusion of chiral molecules. *Soft Matter* **11**, 4167–4172 (2015).
- Jiang, J. & Yang, D. -K. Chirality differentiation by diffusion in chiral nematic liquid crystals. *Phys. Rev. Appl.* **7**, 014014 (2017).
- Morrow, S. M., Bissette, A. J. & Fletcher, S. P. Transmission of chirality through space and across length scales. *Nat. Nanotech.* **12**, 410–419 (2017).
- Santamato, E. et al. Collective rotation of molecules driven by the angular momentum of light in a nematic film. *Phys. Rev. Lett.* **57**, 2423–2426 (1986).
- Murazawa, N. et al. Control of the molecular alignment inside liquid-crystal droplets by use of laser tweezers. *Small* **1**, 656–661 (2005).
- Choi, H. & Takezoe, H. Circular flow formation triggered by Marangoni convection in nematic liquid crystal films with a free surface. *Soft Matter* **12**, 481–485 (2016).

28. Lehmann, O. Struktur, system und magnetisches verhalten flüssiger krystalle und deren mischbarkeit mit festen. *Ann. Phys.* **307**, 649–705 (1900).
29. Ignes-Mullo, J., Poy, G. & Oswald, P. Continuous rotation of achiral nematic liquid crystal droplets driven by heat flux. *Phys. Rev. Lett.* **117**, 057801 (2016).
30. Tabe, Y. & Yokoyama, H. Coherent collective precession of molecular rotors with chiral propellers. *Nat. Mater.* **2**, 806–809 (2003).

Acknowledgements

This research was supported financially by the H2020-MSCA-IF-2014 programme (Grant 661315 to T.O.), the Netherlands Organization for Scientific Research (FOM Grant 13PR3105 to F.L. and N.K.), and the European Research Council (Starting Grant 307784 to N.K.).

Author contributions

E.B. and N.K. initiated and guided the research. The laser experiments were designed by E.B. and performed by T.O. and C.L. The light-responsive liquid crystals were

designed by N.K. and prepared by F.L. and S.I. S.I. synthesized the molecular motors. E.B. conceived the model. E.B. and T.O. performed the simulations. E.B., N.K., T.O. and F.L. analysed the data and discussed the results at all stages. E.B. and N.K. wrote the manuscript.

Competing interests

The authors declare no competing financial interests.

Additional information

Supplementary information is available for this paper at <https://doi.org/10.1038/s41565-017-0059-x>.

Reprints and permissions information is available at www.nature.com/reprints.

Correspondence and requests for materials should be addressed to N.K. or E.B.

Publisher's note: Springer Nature remains neutral with regard to jurisdictional claims in published maps and institutional affiliations.

Methods

Synthesis of the motors and shape-persistent dopants. The detailed synthesis of Ph-**m** and Me-**m**, as well as their purification, are described in the Supplementary Information (for synthetic schemes, see Supplementary Schemes 2 and 3, for NMR characterization, see Supplementary Figures 6–9). The shape-persistent dopant 2,2'-(1,3-propylenedioxy)-1,1'-binaphthalene was synthesized by using known procedures³¹.

Characterization of the motors and shape-persistent dopants. Helical twisting powers (HTP) were measured in the nematic liquid crystal E7 (Merck), by using the Grandjean–Cano wedge method. For each motor enantiomer this yielded the following values: (S,P)-Ph-**m** HTP_{wt%} = +92 μm⁻¹, (R,M)-Ph-**m** HTP_{wt%} = -92 μm⁻¹, (R,P)-Me-**m** HTP_{wt%} = +46.3 μm⁻¹, (S,M)-Me-**m** HTP_{wt%} = -65.1 μm⁻¹. The HTPs of the shape-persistent dopants were (R)-BB HTP_{wt%} = -60.2 μm⁻¹ and (S)-BB HTP_{wt%} = +60.3 μm⁻¹. These values were used to prepare cholesteric liquid crystals with adequate photo-responsive behaviour.

Preparation of the photo-responsive cholesteric liquid crystals. One given enantiomer of molecular motor **m** and the BB enantiomer with opposite helical twisting power were dissolved in the commercially available liquid crystal E7 (Merck Japan), in proportions that are determined by using the equation $p = \Sigma_i (\text{HTP}_i, c_i, ee_i)^{-1}$, where c_i is the concentration of the i th dopant, and ee_i its enantiomeric purity (this equation is valid only at low concentrations). By using this dependence of the helical pitch to the concentration of dopants, it is possible to pre-program the handedness of the cholesteric helix under irradiation (Supplementary Table 1).

For each photo-responsive cholesteric liquid crystal, the value of the pitch was measured before illumination and at the photo-stationary state under uniform illumination with sufficiently high intensity by means of the Cano–Grandjean wedge method, with a wedge angle α defined by $\tan(\alpha) = 0.0269$. The handedness of the cholesteric helix was determined using a known procedure³².

Further, the liquid crystal was placed into a glass cell of thickness $L = 10 \mu\text{m}$ that consists of two parallel substrates providing perpendicular orientation for the liquid crystal molecules (E.H.C. Tokyo). The relaxation time of the cholesteric helix from p_∞ to p_0 was determined by monitoring the sample between crossed linear polarizers.

Simplified reaction–diffusion model before spontaneous symmetry breaking.

A simplified analytical model is presented for the light-induced formation of the precursor of the revolving chiral patterns. The model is based on the assumption of a simple reaction scheme: a molecular motor **m** with an absorption coefficient ϵ absorbs a photon of light with intensity I at $\lambda = 375 \text{ nm}$, and photo-chemically transforms into **m*** with a quantum yield ϕ . At the same time, **m*** undergoes a spontaneous reverse conversion into **m**, characterized by a characteristic relaxation time τ . Regarding the diffusion process, we consider the framework of axisymmetric irradiation profile and axisymmetric concentration profiles for the motors **m** and **m***, c and c^* , respectively. In a first approximation, we neglect the coupling to the liquid crystalline structure and assume the same diffusion constant D_0 for all motors. Assuming no degradation of the motors, this implies that the sum of c and c^* is constant and equals the initial concentration c_0 of the isomer **m**. Finally, neglecting light intensity depletion along the z coordinate as light passes through the liquid crystal layer, the reaction–diffusion equation for $c = c(r, t)$ is expressed as

$$\frac{dc}{dt} = -I\epsilon\phi c + \frac{c_0 - c}{\tau} + D_0 \Delta c \quad (1)$$

After the steady state is reached, namely for $t \gg \tau$, the dynamical equilibrium is characterized by the inhomogeneous intensity-dependent concentration

$$c(r) = \lim_{t \gg \tau} c(r, t) \quad (2)$$

When introducing the dimensionless radius $\rho = r / \sqrt{\tau D_0}$, the steady-state concentration profile $c(\rho)$ satisfies the following differential equation:

$$\frac{d^2 c}{d\rho^2} + \frac{1}{\rho} \frac{dc}{d\rho} - (1 + \tilde{I}(\rho))c + c_0 = 0 \quad (3)$$

with the boundary conditions

$$\left. \frac{dc}{d\rho} \right|_{\rho=0} = 0, \quad \lim_{\rho \rightarrow \infty} c = c_0 \quad (4)$$

where a reduced light intensity profile has been introduced, namely

$$\tilde{I}(\rho) = I(\rho) / I_s \quad (5)$$

$$\text{with } I_s = 1 / (\epsilon\phi\tau) \quad (6)$$

From non-uniform molecular motors concentration to spatially varying cholesteric pitch. The pitch p of a cholesteric liquid crystal prepared by dissolving a few percent of chiral dopants in a nematic liquid crystal satisfies, in the absence of intermolecular interactions between the chiral molecules and assuming enantiopure compounds,

$$p^{-1} = \beta c + \beta^* c^* + \beta_{\text{BB}} c_{\text{BB}} \quad (7)$$

where β and β^* are the HTPs of the **m** and **m***, and β_{BB} and c_{BB} are the HTP and concentration of the shape-persistent chiral dopant. The latter expression can be simplified by introducing the steady-state pitch values at rest, $\tilde{I} = 0$, and in the saturated regime, $\tilde{I} \gg 1$, namely p_0 and p_∞ , respectively, that are given by the expressions

$$p_0^{-1} = \beta c_0 + \beta_{\text{BB}} c_{\text{BB}} \quad (8)$$

$$p_\infty^{-1} = \beta^* c_0 + \beta_{\text{BB}} c_{\text{BB}} \quad (9)$$

Then, accounting for the condition

$$c + c^* = c_0 \quad (10)$$

we get the following expression for the intensity-dependent pitch profile

$$p^{-1} = p_0^{-1} \frac{c}{c_0} + p_\infty^{-1} \left(1 - \frac{c}{c_0} \right) \quad (11)$$

Finally, we introduce the critical pitch $p_c = 2k_2 L$ above which the cholesteric film is frustrated, where L is the cell thickness and $k_2 = K_2 / K_3$ the ratio between twist and bend Frank elastic constants. In Fig. 4c, $p_0 > 0$ and $p_\infty > 0$ (blue curve) or $p_\infty < 0$ (red curve). The radial dependence is obtained by taking into account the Gaussian intensity profile of the light beam

$$I = I_0 \exp(-2r^2 / w^2) \quad (12)$$

Extracting parameters from the experimental data using a simple reaction–diffusion model.

Although the simplified model presented above cannot predict the broken axial symmetry, the two unknown parameters of the model, I_s and D_0 , can be nevertheless determined from experimental observations. Noticeably, I_s represents the combination of coefficients describing the photo-chemical isomerization of **m** to **m*** and its backward thermal relaxation; its value is fixed for a given composition of the cholesteric liquid crystal. Thus, first the experimental data on P_{min} and d_{min} observed in a given sample are used in the model to estimate the value of I_s (Supplementary Fig. 4a). Second, the diameter of twisted pattern as a function of the total beam power is calculated using the obtained I_s value and compared with the experimental plots (Supplementary Fig. 4b). Implementing this two-step procedure for all the samples, the range for molecular diffusion coefficient D_0 covering the experimental data is found. For the relaxation time, we use the values τ (Ph-**m**) = 1,000 s and τ (Me-**m**) = 330 s³³. The resulting range for D_0 is 10^{-11} – $10^{-10} \text{ m}^2 \text{ s}^{-1}$. Changes in the spatial radial distributions of **m** and **m*** concentrations depending on the diffusion coefficient demonstrate the effect of molecular diffusion on the system (Supplementary Fig. 5).

Data availability. The data that support the plots within this paper and other findings of this study are available from the corresponding authors upon reasonable request.

References

- van Es, J. J. G. S., Biemans, H. A. M. & Meijer, E. W. Synthesis and characterization of optically active cyclic 6,6'-dinitro-1,1'-binaphthyl-2,2'-diethers. *Tetrahedron* **8**, 1825–1831 (1997).
- Gerber, P. R. On the determination of the cholesteric screw sense by the Grandjean–Cano-method. *Z. Nat.* **35**, 619–622 (1980).
- Aßhoff, S. J. et al. Time-programmed helix inversion in phototunable liquid crystals. *Chem. Commun.* **49**, 4256–4258 (2013).